CETP inhibitor evacetrapib enters mouse brain tissue

Jasmine Phénix[1,4*], Jonathan Côté[2,3*], Denis Dieme[2,3], Sherilyn J Recinto[1,4,5], Felix Oestereich[1,4,5], Sasen Efrem[1,4], Sami Haddad[2,3#], Michèle Bouchard[2,3#], Lisa Marie Munter[1,4#]

[1] Department of Pharmacology and Therapeutics, McGill University, 3649 Promenade Sir William Osler, Montreal, Quebec, Canada H3G 0B1

[2] Department of Environmental and Occupational Health, School of Public Health, Université de Montreal, Montreal, Quebec, Canada

[3] Public Health Research Center (CReSP), Université de Montréal, Montreal, Quebec, Canada.

[4] Cell Information Systems group, Bellini Life Sciences Complex, 3649 Promenade Sir William Osler, Montreal, QC, Canada H3G 0B1

[5] Integrated Program in Neuroscience, McGill University, Montréal, QC, Canada H3A 2B4

*These Authors contributed equally to the work.

[#]Co-corresponding authors:

Sami Haddad, PhD, sami.haddad@umontreal.ca, Université de Montreal, Department of Environmental and Occupational Health, Roger-Gaudry local U-407, 7101 avenue du Parc, Montreal, QC, Canada, H3N 1X9

Dr. Michèle Bouchard, PhD, michele.bouchard@umontreal.ca, Université de Montreal, Department of Environmental and Occupational Health, Roger-Gaudry local U-424, 7101 avenue du Parc, Montreal, QC, Canada, H3N 1X9

Dr. Lisa Munter, lisa.munter@mcgill.ca, McGill University, Department of Pharmacology and Therapeutics, Bellini Life Sciences Complex, 3649 Promenade Sir-William Osler, Montreal, QC, Canada, H3G 0B1

Abstract

High levels of plasma cholesterol, especially high levels of low-density lipoprotein-cholesterol (LDL-C), have been associated with an increased risk of Alzheimer's disease. The cholesteryl ester transfer protein (CETP) in plasma distributes cholesteryl esters between lipoproteins and increases LDL-C in plasma. Epidemiologically, decreased CETP activity has been associated with sustained cognitive performance during aging, longevity, and a lower risk of Alzheimer's disease. Thus, pharmacological CETP inhibitors could potentially be repurposed for the treatment of Alzheimer's disease as they are safe and effective at lowering CETP activity and LDL-C. While CETP is mostly expressed by the liver and secreted into the bloodstream, CETP is also expressed by astrocytes in the brain. It is therefore important to determine if CETP inhibitors can enter the brain. Here, we describe pharmacokinetic parameters of the CETP inhibitor evacetrapib in plasma, liver, and brain tissues in CETP transgenic mice. We show that evacetrapib crosses the blood-brain barrier and is detectable in brain tissue 0.5 h after a 40 mg/kg i.v. injection in a nonlinear function. We conclude that evacetrapib may prove to be a good candidate to treat CETP-mediated cholesterol dysregulation in Alzheimer's disease.

Introduction

Cholesterol plays major roles in diverse processes essential to life and is ubiquitously found in membranes and organelles in mammalian cells[1, 2]. Cholesterol acts as a signal transducer for many signaling pathways and is the precursor for steroid hormones[3-6]. Though cholesterol is necessary for proper development and maintaining homeostasis, dysregulated cholesterol metabolism has also been shown to be associated with a plethora of pathologies from cardiovascular diseases to neurodegenerative diseases including Parkinson's disease, amyotrophic lateral sclerosis, and Alzheimer's disease[7-10]. Interestingly, higher levels of plasma cholesterol and LDL-C were also associated with an increased risk of developing Alzheimer's disease[7, 11, 12]. However, the molecular mechanisms by which peripheral LDL-C may increase the risk for Alzheimer's disease remain unclear, especially since LDL particles do not cross the blood-brain-barrier[13].

The cholesteryl ester transfer protein (CETP) is a plasma glycoprotein mostly secreted by the liver, spleen, adipose tissues, and brain[14]. Its main function is to mediate the transport of cholesteryl esters and triglycerides between plasma lipoproteins. The CETP transporter works according to a

concentration gradient leading to a net flux of cholesteryl esters from high-density lipoproteins (HDL) particles into LDL and very low-density lipoproteins (VLDL), thus increasing the total LDL-C and VLDL-C levels in the plasma[15]. To treat lipid-related diseases with minimal side-effects, CETP inhibitors were proposed as a new class of non-statin cholesterol-lowering drugs to increase HDL-C and decrease LDL-C in plasma. Therefore, several CETP inhibitors such as dalcetrapib (Hoffman-La Roche)[16], anacetrapib (Merck)[17] and evacetrapib (Eli Lilly)[18] or obicetrapib (Dezima Pharma)[19] have been developed and have been tested in phase III clinical trials for the prevention of cardiovascular disease[20]. While the first generation of CETP inhibitors like torcetrapib (Pfizer)[21] did have off-target effects, all subsequently developed CETP inhibitors were demonstrated to be safe and proven to be effective at lowering LDL-C while raising HDL-C to varying extents. However, they failed to reduce cardiovascular events over already existing drugs and thus were not approved for the treatment of cardiovascular disease[20, 22]. Nevertheless, CETP inhibitors may carry potential for being repurposed in other conditions such as Alzheimer's disease.

A connection between dementia and CETP has been reported in several studies[23-25]. Certain polymorphisms close to or within the *CETP* gene were found to be associated with good cognitive performance and modified the risk of developing Alzheimer's disease[24, 26, 27]. In a Spanish patient cohort, the *CETP* polymorphism rs1800775 (629A) reduced CETP lipid transfer activity by 21-51% as compared to wild type CETP and was associated with a lower risk of Alzheimer's disease in patients expressing the apolipoprotein E isoform 4 (APOE4)[18]. APOE4 plays an important role in lipoprotein-mediated lipid transport and interestingly the ε4 allele represents the greatest known genetic risk factor for late-onset Alzheimer's disease[28, 29]. Furthermore, the CETP polymorphism rs5882 (I405V) was correlated with lower CETP protein expression and higher HDL-C levels and was significantly associated with exceptional longevity and healthy aging in the Ashkenazi Jewish centenarians[23, 25]. Thus, the association between CETP serum activity, and possible interactions with APOE underlines the therapeutic value of targeting CETP to maintain healthy aging, prevent Alzheimer's disease and increase longevity[24]. As such, the use of CETP inhibitors may positively impact cognitive performance, promote longevity, and modulate the risk of Alzheimer's disease potentially through cholesterol-dependent mechanisms.

To evaluate the potential of CETP inhibitors for Alzheimer's disease prevention, preclinical modeling in mice is necessary. Of note, mice do not express CETP or any orthologous genes and as a result, mice have naturally very low LDL levels, thereby limiting the use of such rodents in investigating LDL-related diseases. Therefore, transgenic mice expressing the human *CETP* gene (*hCETPtg*) were developed in 1991 and have since widely been used in cardiovascular disease research[30, 31]. hCETPtg mice have demonstrated a similar CETP expression pattern to humans, and most importantly, on a high cholesterol diet they show elevated LDL plasma levels comparable to those of healthy individuals[32]. In humans, CETP is mostly expressed in the liver and secreted to the plasma but has also been found in the cerebrospinal fluid at 12% of the concentration found in the plasma, as well as in the brain. As plasma CETP does not cross the blood-brain barrier, this suggests direct synthesis of CETP within the brain[33, 34]. Indeed, our laboratory previously confirmed *CETP* mRNA expression in astrocytes enriched from hCETPtg mouse brains[35]. The functions carried out by cerebral CETP remain unclear, since only HDL-like particles are formed in the brain and there are no LDL-like particles. Thus, the question as to whether CETP of the brain or of the periphery modulates the risk of Alzheimer's disease prevails. To first assess if the potent CETP inhibitor evacetrapib can reach brain tissue, we herein characterized the pharmacokinetics of evacetrapib in hCETPtg mice.

Materials and Methods:

Chemicals

Evacetrapib was purchased from Adooq Biosciences (USA). All other reagents were commercially available and were pure or liquid chromatography/mass spectrometry (LC/MS) grade.

Animal acclimatation and housing

hCETPtg mice with a C57BL/6J background were chosen as the experimental model (Jackson Laboratory). Mice were housed in the Goodman Cancer animal facility (12-h light-dark cycle; 20-26°C and 40-60% humidity) in polysulfone cages of two to five mice per cage. Husbandry was heterozygous and mice were genotyped by Transnetyx™, at 3 weeks of age. The protocol was approved by the Animal Compliance Office from the McGill University (ACO approval# 2013-7359).

Animal exposure and sample collection

The experiment was carried out in conformity with the OECD Guidelines 497. Male hCETPtg mice were chosen for the pharmacokinetic analysis. Mice were fed Teklad Global Diets #2018 from Envigo, Canada, for 8 weeks starting from birth followed by a diet change of Modified Low-Fat RD Western diet to match TD.08485 with 1% cholesterol from Research Diets #D16121201 for a duration of three to four weeks. Throughout that period, tap water was provided *ad libitum*. Initially, evacetrapib was solubilized in 20% of the final solution volume of Kolliphor® EL (pH-range 6.0-8.0 cat# C5135) by alternating between 5-minute intervals using an ultrasonic water bath at 4°C and hot water bath at 50°C until complete dissolution. Then, 80% of the final volume was added (isotonic glucose solution 50 g/L glucose containing D-(+)-glucose Sigma cat# G7021 in MilliQ water, sterile filtered).

CETP inhibitor evacetrapib was administered through tail vein injection at doses of 40 mg/kg bodyweight (BW) or 120 mg/kg BW. Mice weighed 28.42 ± 3.16 g on the day of injections. Mice were randomly divided into two groups: 24 mice received a dose of 40 mg/kg BW of evacetrapib while 24 other mice received a dose of 120 mg/kg BW. Mice from both groups were sacrificed at 0, 0.5, 2, 6, 12, and 24 h post injection. Mice sacrificed at later time points had continued access to food and water until the end of the experiment. Blood was collected (300-500 µL) at sacrifice for each mouse by cardiac puncture. Blood plasma was extracted using 10 µL of 1 M EDTA pH 8.0 solution in MilliQ water. Brain and liver tissues were collected immediately after sacrifice, rinsed in 0.9% NaCl solution, and snap-frozen in liquid nitrogen. Samples were stored at -80°C until analysis.

UHPLC-MS-qTOF analysis

Sample preparation and digestion for evacetrapib analysis was performed by UHPLC-MS-qTOF. Working solutions from a stock of evacetrapib were prepared at concentrations of 10 µmol, 100 nmol, 1 nmol, 500 pmol, and 125 pmol per mL of methanol. Working solutions of anacetrapib used as an internal standard was prepared at concentrations of 10 µmol, 100 nmol, 1 nmol per mL from a stock solution.

Brain and liver samples were homogenized using a polytron supplemented with a carbonate buffer at pH 9.8. The volume was adjusted such that each sample reached a final concentration of 100 mg/mL of buffer. A volume of 0.5 mL of homogenate was transferred to a pyrex tube and enriched with 100 µL of 1 nmol/mL anacetrapib solution used as an internal standard. Then, samples were extracted twice using 4 mL of saturated ethyl acetate. For each extraction, samples were shaken for 30 min using a lateral shaker followed by a centrifugation round (20 min, 3000 rpm, 4°C). Organic phases were collected and combined, then evaporated until dry under nitrogen stream in a rotating bath at 40°C. The residues were resuspended in 500 µL and 300 µL of methanol for the liver and the brain, respectively. To fully dissolve the residues, samples were vortexed until no residues were left. Resuspended residues for both brain and liver were then centrifuged (20 min, 3000 rpm, 4°C). The supernatant was recovered, transferred into new vials, and injected into the UHPLC-MS-qTOF.

For the plasma measurement, 20 µL of plasma was enriched with 100 µL of 1 nmol/mL anacetrapib solution in a microtube. A volume of 200 µL of ethanol was added to each sample and vortexed for 30 seconds followed by an incubation period (30 min, 22°C). Samples were then centrifuged (5 min, 16000 g, 10°C). The supernatant was collected and transferred to another microtube. The remaining phase was then mixed with 200 µL of ethanol and resuspended, vortexed for 30 seconds followed by an incubation period (30 min, 22°C) for a second time. Samples were centrifuged (5 min, 16000 g, 10°C) and the supernatant was collected and pooled with the previous extract. To separate the liquid phase from the solid phase, samples were dried under a gentle nitrogen stream. The residues were subsequently dissolved in 500 µL of methanol and vortexed. To fully dissolve the residues, samples were vortexed until no residues were left. Resuspended residues for the plasma were then centrifuged (20 min, 3000 rpm, 4°C). The supernatant was recovered, transferred into new vials, and injected into the UHPLC-MS-qTOF.

The UHPLC-MS-qTOF system consisted of an Agilent model 1290-LC binary gradient UHPLC system (Agilent, Mississauga, Canada) connected to an Agilent model 1290 autosampler and thermostated column compartment (Agilent, Mississauga, Canada) and coupled to a quadrupole time-of-flight mass spectrometer with a Dual J et Stream Electrospray Ionization (Dual-AJS ESI) source (Agilent Technologies, Mississauga, Ontario, Canada). The AJS ESI interface was operated

in positive ion mode. The column used was an Agilent Zorbax Eclipse plus C18 (2.1 x 50 mm; 1,8 µm). The precolumn used was Agilent *Fast Guard* Zorbax Eclipse plus C18 (2.1 X 5 mm; 1,8 µm). HPLC elution solutions were H_2O eluant 0.01% acidified (1 L ultra-pure water + 100 µL of HPLC-grade acetic acid) and methanol eluant 0.01% acidified (1 L MS-grade methanol + 100 µL HPLC-grade acetic acid). Tuning of the instrument was performed once a month and a calibration was performed once a week to accurately analyze the mass ratio m/z < 1700.

The exact mass of evacetrapib was determined in MS mode using the following ToF conditions: sheath gas (N2) temperature at 365°C and gas flow rate of 10 L/min; nebulizer gas pressure of 50 psi; drying gas temperature (N2) at 200°C and flow rate of 12 L/min; capillary voltage (Vcap) at 3000 V, nozzle voltage at 1000 V, fragmentor at 75 V, skimmer at 65 V and octopole at 750 V. The precursor ion $[M+H]^+$ evacetrapib of analyzed was m/z 639.28797. Identification and quantification were performed in Extracted Ion Chromatogram (EIC) mode.

Quantification was carried out using a seven-point-calibration curve with internal standard correction, prepared respectively in brain, liver or in plasma. These curves were established by plotting the response factors as a function of the concentration levels, over a maximum range of 6.25 to 200 pmol/mL. The response factors corresponded to the peak-area ratios of evacetrapib ion to the anacetrapib internal standard ion. The limit of detection (LOD) (corresponding to 3 times of standard deviations of response ratio from replicate analysis of a blank) were 30.3 pmol/g of brain, 11.5 pmol/g of liver and 83 pmol/mL of plasma. Repeatability from replicate analysis of samples under the same calibration and tuning conditions (blank samples spiked with evacetrapib standards at two levels) was below 5%. The recovery percentages determined in the different matrices with two levels of spikes were between 95 and 108%.

Data analysis and determination of main kinetic parameters from different organ time courses

The time courses of evacetrapib in blood, brain, and liver were established following injection of 40 and 120 mg/kg BW in mice (expressed as the average concentration in nmol/mL or nmol/g over time). The parameters used to determine the fit come the following equation $A_1e^{(b_1*t)} + A_2e^{(b_2*t)}$ where A_1 and A_2 are, the different intercepts within the function and b_1 and b_2 are the different slopes within the function, and t is the specific time for which the parameter is calculated. The

concentration-time course data for each tissue was independently fitted with Microsoft Excel using the solver function set on the generalized reduced gradient (GRG) nonlinear method. Using the parameters generated by the fit, the slope and intercepts were determined. The elimination rate constant k_i and the half-life ($t_{1/2}$) for each tissue at both concentrations were calculated using the following equations:

$$ki = -slope \quad [1]$$

$$t_{\frac{1}{2}} = \frac{ln_2}{k} \quad [2]$$

Pharmacokinetic parameters such as area under the plasma concentration-time curve (AUC_{IV}), area under the first moment of the plasma concentration-time curve from time zero to infinity ($AUMC_{IV}$), mean residence time (MRT), apparent total body clearance of the drug from plasma (CL_{blood}) and apparent volume of distribution at steady state (Vss) were determined using the following equations:

$$AUC_{IV} = \frac{1}{2}\sum_{\forall i}(t_i - t_{i-1})[C(t_i) + C(t_{i-1})] \quad [3]$$

$$AUMC_{IV} = \frac{1}{2}\sum_{\forall i}(t_i - t_{i-1})[t_i C(t_i) + t_{i+1} C(t_{i-1})] \quad [4]$$

$$MRT = \frac{AUMC_{IV}}{AUC_{IV}} \quad [5]$$

$$Cl_{blood} = \frac{Dose_{IV}}{AUC_{IV}} \quad [6]$$

$$Vss = Cl_{blood} \times MRT_{IV} \quad [7]$$

Mice were not perfused at sacrifice to allow for plasma, brain, and liver to be collected accurately at time point 0 and uniformly across all time points. Thus, residual blood in vessels of the brain may have left residual traces of evacetrapib in brain samples. Residual plasma volume in mouse brains was determined to be on average 8 µL according to a study by Kaliss[36]. The quantity of evacetrapib in a volume of 8 µL of plasma was calculated using the average concentration in the plasma for each time point (in nmol/mL) multiplied by the volume. The literature shows that the conversion ratio of gram of brain to milliliter of brain is 1.04 mL for each gram[37]. Using the average concentration of evacetrapib (in nmol/g) in the brain and the average brain volume per gram, the average concentration (in nmol/mL) was calculated for each time point. From the calculated average concentration of evacetrapib in the brain (in nmol/mL), the quantity of

evacetrapib (in nmol) in the brain for each time point was determined. Subtracting the amount of previously calculated average concentration of evacetrapib in the residual blood (in nmol/mL) to the average amount of evacetrapib in the brain for each time point (in nmol/mL), the average concentration of evacetrapib in the brain was corrected for residual blood (in nmol/mL and converted back to nmol/g).

Following the correction for the evacetrapib amount in the residual blood in the brain samples - using the area under the curve (AUC in nmol x h/mL) in the brain divided by the area under the curve in the plasma - the plasma-to-brain-tissue penetration ratio was calculated to determine the extent of which evacetrapib is detected in the brain depending on the initial concentration. The tissue penetration ratio allows to approximate how much evacetrapib is accumulated in the brain and whether it is consistent with dosage given to mice. The equation used to calculate this parameter is:

$$Penetration\ ratio\ = \frac{AUC_{IV\ brain}}{AUC_{IV\ plasma}} \quad [8]$$

Distribution to brain

To obtain more mechanistic information on the distribution of evacetrapib to the brain, a semi-physiological-based pharmacokinetic (PBPK) model was developed. First, a two-compartmental model (*i.e.*, a plasma and a peripheral compartment) with a first order elimination rate was fitted to describe the compound's kinetic in plasma (Figure 1). Second, a third compartment was added and connected to the plasma compartment (Figure 1). The parameters related to the brain compartment are presented Table 1. The brain compartment was subdivided into vascular and tissue sub-compartments, with mass balance differential equations describing a distribution in the tissue that can be limited by diffusion as follows:

$$\frac{dA_{BrT}}{dt} = PA \cdot C_{BrP} - PA \cdot {}^{C_{BrT}}/_{P_{Br}} \quad [9]$$

$$C_{BrT} = {}^{A_{BrT}}/_{V_{Br}(1 - V_{Br}F)} \quad [10]$$

$$\frac{dA_{BrP}}{dt} = Q_{Br}\left(C_p - C_{BrP}\right) - \left(PA \cdot C_{BrP} - PA \cdot {}^{C_{BrT}}/_{P_{Br}}\right) \quad [11]$$

$$C_{BrP} = {A_{BrP}}/{(V_{Br} \cdot V_{Br}F \cdot PF)} \quad [12]$$

$$C_{Br} = \frac{A_{BrV}+A_{BrP}}{V_{Br}} \quad [13]$$

where A_{BrT} : amount in brain tissue;

A_{BrV} : amount in brain vascular subcompartment;

C_{BrV} : concentration in brain vascular subcompartment;

C_{BrT} : concentration in brain tissue subcompartment;

C_p : plasma concentration;

PA : permeability area product;

$P_{Br:}$: brain-to-plasma partition coefficient;

PF : plasma fraction of blood;

Q_{Br} : plasma flow to brain.

Using this semi-PBPK model and brain concentration data, several scenarios were tested to see what mechanisms best explain accumulation in the brain : 1) no permeability (i.e., PA=0 L/h); 2) a perfusion limited distribution (PA > 1,000,000 L/h) using the predicted P_{Br}; 3) a perfusion limited distribution with a low P_{Br} (fitted); 4) a diffusion limited distribution (fitted PA) with using the predicted P_{Br}; 5) diffusion limited distribution (fitted PA) and a low P_{Br} (fitted).

Results

Plasma elimination of evacetrapib

For both mice cohorts administered evacetrapib at 40 and 120 mg/kg BW intravenously, peak plasma values were observed at the first sampling time point t=0 h followed by a rapid distribution phase to different tissues and then a second slower elimination phase from the plasma (Figure 2). Pharmacokinetic parameters were determined based on these blood time courses and are described in Table 1. The drug clearance (CL) from blood of 9.4 mL/h at the 40 mg/kg BW dose was much faster as compared to 3.3 mL/h at the 120 mg/kg BW dose. The mean residence time (MRT) of 2.0 h for the 40 mg/kg BW dose and 1.6 h for the 120 mg/kg BW dose remained similar. The

steady state volume of distribution (Vss) of 18.5 mL was about three-fold greater at the 40 mg/kg BW dose as compared to 5.3 mL for the 120 mg/kg BW dose.

Elimination of evacetrapib in liver

The liver is the primary site for drug metabolism, responsible for the concentration, metabolism and excretion of the majority drugs that pass through the body. As such, evacetrapib quantification was determined in this tissue. For both doses in the liver, the time courses were very similar, showing a steady decrease of evacetrapib over time (Figure 3). Pharmacokinetic parameters were determined and described in Table 1. Results show similar elimination rates of 0.2 h^{-1} for the 40 mg/kg BW dose and 0.3 h^{-1} for the 120 mg/kg BW dose, with the slopes of both curves being parallel to each other. The elimination half-lives of 2.8 h and 2.5 h observed for the 40 mg/kg BW and 120 mg/kg BW, respectively, are of comparable value showing that both doses of evacetrapib are eliminated with the same speed. The MRT was similar for both concentrations (Table 1), though slightly higher for the 40 mg/kg BW indicating that the pharmacokinetic parameters in the liver remain unchanged both in the 40 mg/kg BW and 120 mg/kg BW conditions.

Evacetrapib pharmacokinetics in the brain

To assess whether evacetrapib can enter the brain, evacetrapib concentrations were quantified in this tissue. The time course for both doses shows that indeed evacetrapib enters the brain with a peak concentration after 0.5 h (Figure 4A). To have a more accurate reading of the concentration of evacetrapib in brain tissue, calculations were done to correct for the residual blood in the brain as shown in Table 2 and Figure 4B. For the 40 mg/kg BW dose at time 0 and 24 h, no evacetrapib was present in plasma and thus no correction was performed. At times 0.5, 2, 6, and 12 h, the average concentration of evacetrapib in the brain corrected for residual blood was determined as 1.5, 1.0, 0.5, and 0.1 nmol/g, respectively. For the 120 mg/kg BW dose, the average concentration of evacetrapib corrected for residual blood in the brain at time 0 h was 0 nmol/g. At times 0.5, 2, 6, 12, and 24 h, the average concentration of evacetrapib corrected for residual blood in the brain was determined as 16.7, 15.3, 5.0, 1.0, and 0.02 nmol/g, respectively, in a decreasing manner. This confirms the presence of evacetrapib in the brain tissue starting 30 minutes post-intravenous injection until 12 h post-injection. As reported in Table 1, the MRT values for both evacetrapib concentrations are similar with 3.7 h for the 40 mg/kg BW and 3.4 h for the 120 mg/kg BW dose

showing that similar proportional amounts of evacetrapib enter the brain. Comparing the time courses of evacetrapib for not-corrected (Figure 4A) and corrected (Figure 4B) brain concentrations, the elimination rate constant k and half-lives remained similar, if not identical, for both doses. The MRT remained the same between the brain corrected and not corrected for residual blood in both concentrations as well.

Tissue penetration ratio in the brain

The tissue penetration ratio calculated using the mean AUC (nmol × h/g) of the brain tissue divided by the mean AUC (nmol × h/g) of plasma and accounting for residual blood is described in Table 2 and yielded a ratio of 0.08 for the 40 mg/kg BW and 0.13 for the 120 mg/kg BW dose. Thus, the tissue penetration ratio shows a 1.63-fold increase from the low to the high evacetrapib concentration.

Semi-PBPK model of evacetrapib entering the brain.

We used a semi-physiologic three-compartment model to simulate the *in vivo* data (Figure 1). The parameters for the plasma and peripheral compartments were fitted to the plasma concentration at 40 mg/kg BW (Table 3 and Figure 5b)[38, 39]. Then, four scenarios were simulated against the brain concentration data corrected for residual blood as explained in the method section. When assuming perfusion limited distribution, the model was not able to simulate the observed data (Figure 5a), even when we adjusted for the brain-to-plasma partition coefficient (P_{Br}). However, modeling diffusion limitation in the brain resulted in a better fit of the simulation towards the observed brain concentrations when fitted for the permeability area product (PA) and P_{Br} (Figure 5a, dark grey curve compared to black circles).

Discussion

We investigated the distribution of the CETP inhibitor evacetrapib in hCETPtg mice, and the major finding of this study is that evacetrapib does enter mouse brain tissue. We detected evacetrapib in the brain 0.5 h after intravenous injection at already 40 mg/kg BW in a nonlinear function. Our semi-PBPK compartmental model shows that evacetrapib does not rapidly diffuse across the blood brain barrier indicating that the mechanism of evacetrapib distribution to the brain may rely on facilitated transport mechanisms.

Dysregulation of the cholesterol metabolism has been associated with various diseases such as atherosclerosis[7] and Alzheimer's disease[11, 40]. An important protein regulating the distribution of cholesteryl esters in the blood is CETP, which has been linked to Alzheimer's disease through polymorphisms[24, 26, 27]. Though the function of CETP has mainly been established in the periphery, cholesteryl transfer activity has also been reported in the central nervous system (CNS) and in the cerebrospinal fluid (CSF)[33, 34]. While it has been suggested that plasma cholesterol does not have a direct effect on brain cholesterol levels[13], it remains unclear whether it is CETP activity in the CNS or in the blood that plays a role in dementia. As such, CETP activity and high LDL levels in a given model organism are necessary to assess the potential benefits of evacetrapib *in vivo*. However, unlike humans, mice do not express endogenous CETP, making hCETPtg mice a more representative animal model in terms of peripheral lipoprotein dynamics. Indeed, while wild type mice have very low levels of endogenous LDL, hCETP tg mice have an LDL profile that is much more comparable to humans as a result of CETP activity[32]. We previously found that hCETPtg mice have approximately 22% higher cholesterol content in their brains compared to wild type mouse brains[35]. The elevated cholesterol content in the brain and in the periphery of hCETPtg mice could differentially affect the distribution and elimination kinetics of the very lipophilic CETP inhibitors (evacetrapib has an octanol to water partition coefficient of logP 7.56)[41]. Due to these fundamental physiological differences, pharmacokinetic parameters of a CETP inhibitor should be assessed in hCETPtg mice rather than wild type mice. Thus, hCETPtg mice present a good model for testing CETP inhibitors in the context of drug repurposing for Alzheimer's disease. Remarkably, several proteins associated with Alzheimer's disease are linked to cholesterol. For example, the central protein in Alzheimer's disease, the amyloid precursor-protein (APP), contains cholesterol-binding motifs in its transmembrane sequence[42]. Further proteins encoded by gene variants identified by genome-wide associated studies carry functions related to cholesterol including the most prominent APOE, CLU, SORL1, PICALM, BIN1, SORT1, and ABCA1[29]. As such, CETP may have an indirect modifying role in the Alzheimer's disease by affecting the cholesterol of the brain. Collectively, further investigations are necessary to address the potential impact of CETP inhibition in ameliorating Alzheimer's disease symptoms by reducing cerebral cholesterol.

In addition to seeing whether evacetrapib accumulated in the brain of hCETPtg mice, another important aspect of this study was to determine whether the accumulation of this drug in brain tissue was proportional to the dose received. This had been previously evaluated for another CETP inhibitor dalcetrapib, developed by Hoffman-La Roche, which was also shown to have the capacity to cross the blood-brain barrier of rats[43]. In this study, rats were injected intravenously with 10 mg/kg BW dalcetrapib, which was found to accumulate in the cerebrum and cerebellum up to 24 h post-injection[43]. The greatest amount of dalcetrapib observed in the brain peaked at 2 h after injection, whereas evacetrapib was at its maximum concentration 0.5 h post-injection for both 40 and 120 mg/kg BW doses. Furthermore, the concentration of dalcetrapib measured in the brain of rats at 0.5 h was 21-fold lower than the average concentration of evacetrapib measured at the same time point in mice injected with 120 mg/kg BW, and 2-fold lower than in animals injected with 40 mg/kg BW of evacetrapib. Conversely, at 24 h post-injection, the concentration of dalcetrapib found in the cerebellum and the cerebrum was 16-fold greater than the amount of evacetrapib in the brain of mice injected with 120 mg/kg BW at the same time point, and >20-fold higher than in mice injected with 40 mg/kg BW. Our findings indicate that though evacetrapib may enter the brain tissue faster than dalcetrapib, it has a lower capacity to accumulate and is eliminated faster than dalcetrapib. To our knowledge, whether CETP inhibitor evacetrapib accumulates in the brain with long-term use has not yet been evaluated.

One last factor we considered in this study was the mechanism by which evacetrapib is transported into brain tissue. To that effect, toxicokinetic parameters were derived from the blood and brain time courses, which indicate that the drug possibly requires some sort of transporter to reach peripheral compartments, such as the brain, and in order to clear from brain tissue. The difference in tissue penetration ratio as a function of the dose indicates that a higher concentration of evacetrapib has greater capacity to be detected in brain tissue. A possible explanation could be that evacetrapib enters the brain faster than it is cleared out of it, leading to a buildup in brain tissue. The compartmental model developed suggests that diffusion-limited uptake occurs in the brain[44] and that the P_{Br} was very low, which may indicate that evacetrapib diffuses into the brain inefficiently and would require the use of transporters. To determine which mechanisms are involved in evacetrapib distribution to the brain, a semi-PBPK model was developed (parameter values are in Table 3; Figure 5). To this end, we first aimed to determine the brain:plasma partition

coefficient of evacetrapib using rapid equilibrium dialysis. Our preliminary data showed that the molecule did not appreciably diffuse across the porous membrane; only 2% of evacetrapib diffused after 24 h in the system consisting of plasma on both sides of the membrane. On the one hand, this may be in line with our *in vivo* observations considering that only a small fraction of evacetrapib crossed the blood-brain-barrier. However, the slow diffusion in our *in vitro* model is incongruent to the concentrations of evacetrapib found in the brain 2.2 h following intravenous injections. Thus, the implication of transporters cannot be excluded.

Epidemiological studies indicated that CETP plays a disease-modifying role in Alzheimer's disease[23-25]. While the exact mechanism remains unclear, CETP activity may promote Alzheimer's disease through modifying cholesterol content, distribution, storage, or metabolism, which could potentially be prevented by CETP inhibitors such as evacetrapib. To set the grounds to assess CETP inhibitors for potential drug repurposing in Alzheimer's disease, we showed here that evacetrapib reaches brain tissue fast after intravenous injection in hCETPtg mice. Furthermore, we demonstrate that evacetrapib crosses to the brain, possibly through the actions of a transporter or other facilitating mechanism. Thus, CETP activity in the brain could be pharmacologically reversed, which may carry the potential to delay or ameliorate Alzheimer's disease.

Acknowledgements: We thank the CMARC Animal Health Technicians for the drug treatments in mice.

Author contributions: JP wrote the manuscript draft, made the figures, bread mice and collected samples after injections. JC modeled the pharmacokinetic parameters. JP and JC performed the pharmacokinetic analysis. DD conducted and analysed evacetrapib detection by mass spectrometry. SJR, SE and FO bread mice and collected mouse samples after injections. SH designed and completed the semi-PBPK model. SH, MB, and LMM designed, coordinated, and supervised the study. All authors revised the manuscript.

Conflicts of Interest: The authors declare no conflict of interest. LMM received funds from New Amsterdam Pharma regarding CETP inhibitors independent from the work presented herein, which was completed in its core prior to this funding.

Funding: This work was funded by the Weston Brain Institute award RR172187, Canadian Institute of Health Research CIHR-PJT-162302, Alzheimer Society of Canada regular Research Grant 17-02, and was supported by the Fonds de Recherche du Québec - Santé FRQS research allocation FRQ-S 36571, the Canada Foundation of Innovation Leaders Opportunity Fund Grant 32565, and Natural Sciences and Engineering Research Council of Canada (NSERC) Discovery Grants RGPIN-2015-04645 to LM. JP and FO received a stipend award by the Canada First Research Excellence Fund, awarded to McGill University for the Healthy Brains for Healthy Lives initiative. JP further received the Laszlo & Etelka Kollar Fellowship of the Faculty of Medicine and Health Sciences of McGill University. FO further received studentships through the Integrated Program in Neuroscience (IPN). SJR received a CGS-Master's award.

Figure legends

Figure 1: Schematic representation of the 3-compartment model simulation for the semi-PBPK model.

Figure 2: Evacetrapib concentration in plasma after a single intravenous injection of evacetrapib at 6 time points over a 24-h course. Symbols represent means ± s.e.m., n=4 per time point.

Figure 3: Evacetrapib concentration in liver after a single intravenous injection of evacetrapib. Symbols represent means ± s.e.m., n=4 per time point.

Figure 4: Evacetrapib concentration in the brain. A) Experimental values not corrected for residual blood. B) Experimental values corrected for residual blood. Symbols represent means ± s.e.m., n=4 per time point.

Figure 5: Semi-PBPK modeling of evacetrapib entering the brain. A) 3-compartment model simulation of the plasma concentration at 40 mg/kg. Experimentally determined values are in black circles. Different perfusion-limited models show different concentrations, with the best fit obtained with diffusion limitation and fitted PA and P_{Br}. B) Parameters for the plasma and peripheral compartments fitted to the plasma concentration at 40 mg/kg BW.

Table 1: Pharmacokinetic parameters of evacetrapib in plasma, liver, and brain. *K: elimination rate constant; $t_{1/2}$: half-life; AUC: area under the curve; AUMC: area under the first moment of the plasma concentration-time curve from time zero to infinity; MRT: mean residence time; CL: drug clearance; Vss: volume of distribution.*

Table 2: Average evacetrapib concentration determined in the brain o*ver a 24-h period after a 40 mg/kg BW and 120 mg/kg BW i.v. injection in hCETP tg mice comparing residual-blood correction to no correction.*

Table 3: Parameter values for the semi physiologically-based pharmacokinetic model *to simulate accumulation in the brain.*

References

[1] Maxfield, F. R., and van Meer, G. (2010) Cholesterol, the central lipid of mammalian cells, *Curr Opin Cell Biol 22*, 422-429.

[2] Paschkowsky, S., Hsiao, J. M., Young, J. C., and Munter, L. M. (2019) The discovery of proteases and intramembrane proteolysis (1), *Biochem Cell Biol 97*, 265-269.

[3] Burke, R., Nellen, D., Bellotto, M., Hafen, E., Senti, K. A., Dickson, B. J., and Basler, K. (1999) Dispatched, a novel sterol-sensing domain protein dedicated to the release of cholesterol-modified hedgehog from signaling cells, *Cell 99*, 803-815.

[4] Porter, J. A., Young, K. E., and Beachy, P. A. (1996) Cholesterol modification of hedgehog signaling proteins in animal development, *Science 274*, 255-259.

[5] Cooper, M. K., Wassif, C. A., Krakowiak, P. A., Taipale, J., Gong, R., Kelley, R. I., Porter, F. D., and Beachy, P. A. (2003) A defective response to Hedgehog signaling in disorders of cholesterol biosynthesis, *Nat Genet 33*, 508-513.

[6] Payne, A. H., and Hales, D. B. (2004) Overview of steroidogenic enzymes in the pathway from cholesterol to active steroid hormones, *Endocr Rev 25*, 947-970.

[7] Whitmer, R. A., Sidney, S., Selby, J., Johnston, S. C., and Yaffe, K. (2005) Midlife cardiovascular risk factors and risk of dementia in late life, *Neurology 64*, 277-281.

[8] Doria, M., Maugest, L., Moreau, T., Lizard, G., and Vejux, A. (2016) Contribution of cholesterol and oxysterols to the pathophysiology of Parkinson's disease, *Free Radic Biol Med 101*, 393-400.
[9] Godoy-Corchuelo, J. M., Fernandez-Beltran, L. C., Ali, Z., Gil-Moreno, M. J., Lopez-Carbonero, J. I., Guerrero-Sola, A., Larrad-Sainz, A., Matias-Guiu, J., Matias-Guiu, J. A., Cunningham, T. J., and Corrochano, S. (2022) Lipid Metabolic Alterations in the ALS-FTD Spectrum of Disorders, *Biomedicines 10*.
[10] Iwagami, M., Qizilbash, N., Gregson, J., Douglas, I., Johnson, M., Pearce, N., Evans, S., and Pocock, S. (2021) Blood cholesterol and risk of dementia in more than 1.8 million people over two decades: a retrospective cohort study, *Lancet Healthy Longev 2*, e498-e506.
[11] Liu, Y., Zhong, X., Shen, J., Jiao, L., Tong, J., Zhao, W., Du, K., Gong, S., Liu, M., and Wei, M. (2020) Elevated serum TC and LDL-C levels in Alzheimer's disease and mild cognitive impairment: A meta-analysis study, *Brain Res 1727*, 146554.
[12] Solomon, A., Kivipelto, M., Wolozin, B., Zhou, J., and Whitmer, R. A. (2009) Midlife serum cholesterol and increased risk of Alzheimer's and vascular dementia three decades later, *Dement Geriatr Cogn Disord 28*, 75-80.
[13] Bjorkhem, I., and Meaney, S. (2004) Brain cholesterol: long secret life behind a barrier, *Arterioscler Thromb Vasc Biol 24*, 806-815.
[14] Tall, A. R. (1995) Plasma Lipid Transfer Proteins, *Annu Rev Biochem 64*, 235-257.
[15] Barter, P., and Rye, K. A. (1994) Cholesteryl ester transfer protein: its role in plasma lipid transport, *Clin Exp Pharmacol Physiol 21*, 663-672.
[16] Ray, K. K., Ditmarsch, M., Kallend, D., Niesor, E. J., Suchankova, G., Upmanyu, R., Anzures-Cabrera, J., Lehnert, V., Pauly-Evers, M., Holme, I., Stasek, J., van Hessen, M. W., Jones, P., and dal, A. I. (2014) The effect of cholesteryl ester transfer protein inhibition on lipids, lipoproteins, and markers of HDL function after an acute coronary syndrome: the dal-ACUTE randomized trial, *Eur Heart J 35*, 1792-1800.
[17] Gotto, A. M., Jr., Kher, U., Chatterjee, M. S., Liu, Y., Li, X. S., Vaidya, S., Cannon, C. P., Brinton, E. A., Moon, J. E., Shah, S., Dansky, H. M., Mitchel, Y., Barter, P., and Investigators, D. (2014) Lipids, safety parameters, and drug concentrations after an additional 2 years of treatment with anacetrapib in the DEFINE study, *J Cardiovasc Pharmacol Ther 19*, 543-549.
[18] Nicholls, S. J., Ray, K. K., Ballantyne, C. M., Beacham, L. A., Miller, D. L., Ruotolo, G., Nissen, S. E., Riesmeyer, J. S., and Investigators, A. (2017) Comparative effects of cholesteryl ester transfer protein inhibition, statin or ezetimibe on lipid factors: The ACCENTUATE trial, *Atherosclerosis 261*, 12-18.
[19] Nicholls, S. J., Ditmarsch, M., Kastelein, J. J., Rigby, S. P., Kling, D., Curcio, D. L., Alp, N. J., and Davidson, M. H. (2022) Lipid lowering effects of the CETP inhibitor obicetrapib in combination with high-intensity statins: a randomized phase 2 trial, *Nat Med 28*, 1672-1678.
[20] Tall, A. R., and Rader, D. J. (2018) Trials and Tribulations of CETP Inhibitors, *Circ Res 122*, 106-112.
[21] Simic, B., Hermann, M., Shaw, S. G., Bigler, L., Stalder, U., Dorries, C., Besler, C., Luscher, T. F., and Ruschitzka, F. (2012) Torcetrapib impairs endothelial function in hypertension, *Eur Heart J 33*, 1615-1624.

[22] Nelson, A. J., Sniderman, A. D., Ditmarsch, M., Dicklin, M. R., Nicholls, S. J., Davidson, M. H., and Kastelein, J. J. P. (2022) Cholesteryl Ester Transfer Protein Inhibition Reduces Major Adverse Cardiovascular Events by Lowering Apolipoprotein B Levels, *Int J Mol Sci 23*.

[23] Barzilai, N., Atzmon, G., Schechter, C., Schaefer, E. J., Cupples, A. L., Lipton, R., Cheng, S., and Shuldiner, A. R. (2003) Unique lipoprotein phenotype and genotype associated with exceptional longevity, *JAMA 290*, 2030-2040.

[24] Rodriguez, E., Mateo, I., Infante, J., Llorca, J., Berciano, J., and Combarros, O. (2006) Cholesteryl ester transfer protein (CETP) polymorphism modifies the Alzheimer's disease risk associated with APOE epsilon4 allele, *J Neurol 253*, 181-185.

[25] Sun, L., Hu, C. Y., Shi, X. H., Zheng, C. G., Huang, Z. Z., Lv, Z. P., Huang, J., Wan, G., Qi, K. Y., Liang, S. Y., Zhou, L., and Yang, Z. (2013) Trans-ethnical shift of the risk genotype in the CETP I405V with longevity: a Chinese case-control study and meta-analysis, *PLoS One 8*, e72537.

[26] Sundermann, E. E., Wang, C., Katz, M., Zimmerman, M. E., Derby, C. A., Hall, C. B., Ozelius, L. J., and Lipton, R. B. (2016) Cholesteryl ester transfer protein genotype modifies the effect of apolipoprotein epsilon4 on memory decline in older adults, *Neurobiol Aging 41*, 200 e207-200 e212.

[27] Lythgoe, C., Perkes, A., Peterson, M., Schmutz, C., Leary, M., Ebbert, M. T., Ridge, P. G., Norton, M. C., Tschanz, J. T., Munger, R. G., Corcoran, C. D., and Kauwe, J. S. (2015) Population-based analysis of cholesteryl ester transfer protein identifies association between I405V and cognitive decline: the Cache County Study, *Neurobiol Aging 36*, 547 e541-543.

[28] Poirier, J., Davignon, J., Bouthillier, D., Kogan, S., Bertrand, P., and Gauthier, S. (1993) Apolipoprotein E polymorphism and Alzheimer's disease, *Lancet 342*, 697-699.

[29] Bellenguez, C., and Kucukali, F., and Jansen, I. E., and Kleineidam, L., and Moreno-Grau, S., and Amin, N., and Naj, A. C., and Campos-Martin, R., and Grenier-Boley, B., and Andrade, V., and Holmans, P. A., and Boland, A., and Damotte, V., and van der Lee, S. J., and Costa, M. R., and Kuulasmaa, T., and Yang, Q., and de Rojas, I., and Bis, J. C., and Yaqub, A., and Prokic, I., and Chapuis, J., and Ahmad, S., and Giedraitis, V., and Aarsland, D., and Garcia-Gonzalez, P., and Abdelnour, C., and Alarcon-Martin, E., and Alcolea, D., and Alegret, M., and Alvarez, I., and Alvarez, V., and Armstrong, N. J., and Tsolaki, A., and Antunez, C., and Appollonio, I., and Arcaro, M., and Archetti, S., and Pastor, A. A., and Arosio, B., and Athanasiu, L., and Bailly, H., and Banaj, N., and Baquero, M., and Barral, S., and Beiser, A., and Pastor, A. B., and Below, J. E., and Benchek, P., and Benussi, L., and Berr, C., and Besse, C., and Bessi, V., and Binetti, G., and Bizarro, A., and Blesa, R., and Boada, M., and Boerwinkle, E., and Borroni, B., and Boschi, S., and Bossu, P., and Brathen, G., and Bressler, J., and Bresner, C., and Brodaty, H., and Brookes, K. J., and Brusco, L. I., and Buiza-Rueda, D., and Burger, K., and Burholt, V., and Bush, W. S., and Calero, M., and Cantwell, L. B., and Chene, G., and Chung, J., and Cuccaro, M. L., and Carracedo, A., and Cecchetti, R., and Cervera-Carles, L., and Charbonnier, C., and Chen, H. H., and Chillotti, C., and Ciccone, S., and Claassen, J., and Clark, C., and Conti, E., and Corma-Gomez, A., and Costantini, E., and Custodero, C., and Daian, D., and Dalmasso, M. C., and Daniele, A., and Dardiotis, E., and Dartigues, J. F., and de Deyn, P. P., and de Paiva Lopes, K., and de Witte, L. D., and Debette, S., and Deckert, J., and Del Ser, T., and Denning, N., and DeStefano, A., and

Dichgans, M., and Diehl-Schmid, J., and Diez-Fairen, M., and Rossi, P. D., and Djurovic, S., and Duron, E., and Duzel, E., and Dufouil, C., and Eiriksdottir, G., and Engelborghs, S., and Escott-Price, V., and Espinosa, A., and Ewers, M., and Faber, K. M., and Fabrizio, T., and Nielsen, S. F., and Fardo, D. W., and Farotti, L., and Fenoglio, C., and Fernandez-Fuertes, M., and Ferrari, R., and Ferreira, C. B., and Ferri, E., and Fin, B., and Fischer, P., and Fladby, T., and Fliessbach, K., and Fongang, B., and Fornage, M., and Fortea, J., and Foroud, T. M., and Fostinelli, S., and Fox, N. C., and Franco-Macias, E., and Bullido, M. J., and Frank-Garcia, A., and Froelich, L., and Fulton-Howard, B., and Galimberti, D., and Garcia-Alberca, J. M., and Garcia-Gonzalez, P., and Garcia-Madrona, S., and Garcia-Ribas, G., and Ghidoni, R., and Giegling, I., and Giorgio, G., and Goate, A. M., and Goldhardt, O., and Gomez-Fonseca, D., and Gonzalez-Perez, A., and Graff, C., and Grande, G., and Green, E., and Grimmer, T., and Grunblatt, E., and Grunin, M., and Gudnason, V., and Guetta-Baranes, T., and Haapasalo, A., and Hadjigeorgiou, G., and Haines, J. L., and Hamilton-Nelson, K. L., and Hampel, H., and Hanon, O., and Hardy, J., and Hartmann, A. M., and Hausner, L., and Harwood, J., and Heilmann-Heimbach, S., and Helisalmi, S., and Heneka, M. T., and Hernandez, I., and Herrmann, M. J., and Hoffmann, P., and Holmes, C., and Holstege, H., and Vilas, R. H., and Hulsman, M., and Humphrey, J., and Biessels, G. J., and Jian, X., and Johansson, C., and Jun, G. R., and Kastumata, Y., and Kauwe, J., and Kehoe, P. G., and Kilander, L., and Stahlbom, A. K., and Kivipelto, M., and Koivisto, A., and Kornhuber, J., and Kosmidis, M. H., and Kukull, W. A., and Kuksa, P. P., and Kunkle, B. W., and Kuzma, A. B., and Lage, C., and Laukka, E. J., and Launer, L., and Lauria, A., and Lee, C. Y., and Lehtisalo, J., and Lerch, O., and Lleo, A., and Longstreth, W., Jr., and Lopez, O., and de Munain, A. L., and Love, S., and Lowemark, M., and Luckcuck, L., and Lunetta, K. L., and Ma, Y., and Macias, J., and MacLeod, C. A., and Maier, W., and Mangialasche, F., and Spallazzi, M., and Marquie, M., and Marshall, R., and Martin, E. R., and Montes, A. M., and Rodriguez, C. M., and Masullo, C., and Mayeux, R., and Mead, S., and Mecocci, P., and Medina, M., and Meggy, A., and Mehrabian, S., and Mendoza, S., and Menendez-Gonzalez, M., and Mir, P., and Moebus, S., and Mol, M., and Molina-Porcel, L., and Montrreal, L., and Morelli, L., and Moreno, F., and Morgan, K., and Mosley, T., and Nothen, M. M., and Muchnik, C., and Mukherjee, S., and Nacmias, B., and Ngandu, T., and Nicolas, G., and Nordestgaard, B. G., and Olaso, R., and Orellana, A., and Orsini, M., and Ortega, G., and Padovani, A., and Paolo, C., and Papenberg, G., and Parnetti, L., and Pasquier, F., and Pastor, P., and Peloso, G., and Perez-Cordon, A., and Perez-Tur, J., and Pericard, P., and Peters, O., and Pijnenburg, Y. A. L., and Pineda, J. A., and Pinol-Ripoll, G., and Pisanu, C., and Polak, T., and Popp, J., and Posthuma, D., and Priller, J., and Puerta, R., and Quenez, O., and Quintela, I., and Thomassen, J. Q., and Rabano, A., and Rainero, I., and Rajabli, F., and Ramakers, I., and Real, L. M., and Reinders, M. J. T., and Reitz, C., and Reyes-Dumeyer, D., and Ridge, P., and Riedel-Heller, S., and Riederer, P., and Roberto, N., and Rodriguez-Rodriguez, E., and Rongve, A., and Allende, I. R., and Rosende-Roca, M., and Royo, J. L., and Rubino, E., and Rujescu, D., and Saez, M. E., and Sakka, P., and Saltvedt, I., and Sanabria, A., and Sanchez-Arjona, M. B., and Sanchez-Garcia, F., and Juan, P. S., and Sanchez-Valle, R., and Sando, S. B., and Sarnowski, C., and Satizabal, C. L., and Scamosci, M., and Scarmeas, N., and Scarpini, E., and Scheltens, P., and Scherbaum, N., and Scherer, M., and Schmid, M., and Schneider, A., and Schott, J. M., and Selbaek, G., and Seripa, D., and Serrano, M., and

Sha, J., and Shadrin, A. A., and Skrobot, O., and Slifer, S., and Snijders, G. J. L., and Soininen, H., and Solfrizzi, V., and Solomon, A., and Song, Y., and Sorbi, S., and Sotolongo-Grau, O., and Spalletta, G., and Spottke, A., and Squassina, A., and Stordal, E., and Tartan, J. P., and Tarraga, L., and Tesi, N., and Thalamuthu, A., and Thomas, T., and Tosto, G., and Traykov, L., and Tremolizzo, L., and Tybjaerg-Hansen, A., and Uitterlinden, A., and Ullgren, A., and Ulstein, I., and Valero, S., and Valladares, O., and Broeckhoven, C. V., and Vance, J., and Vardarajan, B. N., and van der Lugt, A., and Dongen, J. V., and van Rooij, J., and van Swieten, J., and Vandenberghe, R., and Verhey, F., and Vidal, J. S., and Vogelgsang, J., and Vyhnalek, M., and Wagner, M., and Wallon, D., and Wang, L. S., and Wang, R., and Weinhold, L., and Wiltfang, J., and Windle, G., and Woods, B., and Yannakoulia, M., and Zare, H., and Zhao, Y., and Zhang, X., and Zhu, C., and Zulaica, M., and Eadb, and Gr@Ace, and Degesco, and Eadi, and Gerad, and Demgene, and FinnGen, and Adgc, and Charge, and Farrer, L. A., and Psaty, B. M., and Ghanbari, M., and Raj, T., and Sachdev, P., and Mather, K., and Jessen, F., and Ikram, M. A., and de Mendonca, A., and Hort, J., and Tsolaki, M., and Pericak-Vance, M. A., and Amouyel, P., and Williams, J., and Frikke-Schmidt, R., and Clarimon, J., and Deleuze, J. F., and Rossi, G., and Seshadri, S., and Andreassen, O. A., and Ingelsson, M., and Hiltunen, M., and Sleegers, K., and Schellenberg, G. D., and van Duijn, C. M., and Sims, R., and van der Flier, W. M., and Ruiz, A., and Ramirez, A., and Lambert, J. C. (2022) New insights into the genetic etiology of Alzheimer's disease and related dementias, *Nat Genet 54*, 412-436.

[30] Agellon, L. B., Walsh, A., Hayek, T., Moulin, P., Jiang, X. C., Shelanski, S. A., Breslow, J. L., and Tall, A. R. (1991) Reduced high density lipoprotein cholesterol in human cholesteryl ester transfer protein transgenic mice, *J Biol Chem 266*, 10796-10801.

[31] Jiang, X. C., Agellon, L. B., Walsh, A., Breslow, J. L., and Tall, A. (1992) Dietary cholesterol increases transcription of the human cholesteryl ester transfer protein gene in transgenic mice. Dependence on natural flanking sequences, *J Clin Invest 90*, 1290-1295.

[32] Steenbergen, R. H., Joyce, M. A., Lund, G., Lewis, J., Chen, R., Barsby, N., Douglas, D., Zhu, L. F., Tyrrell, D. L., and Kneteman, N. M. (2010) Lipoprotein profiles in SCID/uPA mice transplanted with human hepatocytes become human-like and correlate with HCV infection success, *Am J Physiol Gastrointest Liver Physiol 299*, G844-854.

[33] Albers, J. J., Tollefson, J. H., Wolfbauer, G., and Albright, R. E., Jr. (1992) Cholesteryl ester transfer protein in human brain, *Int J Clin Lab Res 21*, 264-266.

[34] Yamada, T., Kawata, M., Arai, H., Fukasawa, M., Inoue, K., and Sato, T. (1995) Astroglial localization of cholesteryl ester transfer protein in normal and Alzheimer's disease brain tissues, *Acta Neuropathol 90*, 633-636.

[35] Oestereich, F., Yousefpour, N., Yang, E., Phenix, J., Nezhad, Z. S., Nitu, A., Vazquez Coba, A., Ribeiro-da-Silva, A., Chaurand, P., and Munter, L. M. (2022) The cholesteryl ester transfer protein (CETP) raises cholesterol levels in the brain, *J Lipid Res 63*, 100260.

[36] Kaliss, N., and Pressman, D. (1950) Plasma and blood volumes of mouse organs, as determined with radioactive iodoproteins, *Proc Soc Exp Biol Med 75*, 16-20.

[37] Leithner, C., Muller, S., Fuchtemeier, M., Lindauer, U., Dirnagl, U., and Royl, G. (2010) Determination of the brain-blood partition coefficient for water in mice using MRI, *J Cereb Blood Flow Metab 30*, 1821-1824.

[38] Brown, R. P., Delp, M. D., Lindstedt, S. L., Rhomberg, L. R., and Beliles, R. P. (1997) Physiological parameter values for physiologically based pharmacokinetic models, *Toxicol Ind Health 13*, 407-484.
[39] Peyret, T., Poulin, P., and Krishnan, K. (2010) A unified algorithm for predicting partition coefficients for PBPK modeling of drugs and environmental chemicals, *Toxicol Appl Pharmacol 249*, 197-207.
[40] Vance, J. E. (2012) Dysregulation of cholesterol balance in the brain: contribution to neurodegenerative diseases, *Dis Model Mech 5*, 746-755.
[41] Small, D. S., Ke, A. B., Hall, S. D., Mantlo, N., Rotelli, M., and Friedrich, S. (2015) Assessment of the persistence of anacetrapib and evacetrapib concentrations using two pharmacokinetic modeling approaches, *J Clin Pharmacol 55*, 757-767.
[42] Barrett, P. J., Song, Y., Van Horn, W. D., Hustedt, E. J., Schafer, J. M., Hadziselimovic, A., Beel, A. J., and Sanders, C. R. (2012) The amyloid precursor protein has a flexible transmembrane domain and binds cholesterol, *Science 336*, 1168-1171.
[43] Takubo, H., Ishikawa, T., Kuhlmann, O., Nemoto, H., Noguchi, T., Nanayama, T., Komura, H., and Kogayu, M. (2014) Pharmacokinetics and disposition of dalcetrapib in rats and monkeys, *Xenobiotica 44*, 1117-1126.
[44] Poulin, P., and Haddad, S. (2011) Microsome composition-based model as a mechanistic tool to predict nonspecific binding of drugs in liver microsomes, *J Pharm Sci 100*, 4501-4517.

Table 1: Pharmacokinetic parameters of evacetrapib in plasma, liver, and brain.
K: elimination rate constant; t1/2: half-life; AUC: area under the curve; AUMC: area under the first moment of the plasma concentration-time curve from time zero to infinity; MRT: mean residence time; CL: drug clearance; Vss: volume of distribution

	Mean values of the pharmacokinetic parameters after 24h						
	Organ	Plasma		Brain		Liver	
Pharmacokinetic parameter	Dose (mg/kg BW)	40	120	40	120	40	120
K_α (h^{-1})		6.5	1.8	-	-	-	-
$t_{1/2\alpha}$ (h)		0.1	0.4	-	-	-	-
K_β (h^{-1})		0.4	0.2	0.2	0.3	0.2	0.2
$t_{1/2\beta}$ (h)		2.3	3.0	2.8	2.5	3.0	3.2
AUC (nmol × h/mL)		203	1418	10.6	115	267	881
AUMC (nmol × h^2/mL)		398	2297	39.2	395	1183	3167
MRT (h)		2.0	1.6	3.7	3.4	4.4	3.6
CL (mL/h)		9.4	3.3	-	-	-	-
Vss (mL)		18.5	5.3	-	-	-	-

Table 2: Average evacetrapib concentration determined in the brain over a 24-h period after a 40 mg/kg BW and 120 mg/kg BW i.v. injection in hCETP tg mice comparing residual-blood correction to no correction.

	Concentration of evacetrapib in the brain for 40 mg/kg BW dose (mean ± SD)			Concentration of evacetrapib in the brain for 120 mg/kg BW dose (mean ±SD)		
	Measured	Calculated		Measured	Calculated	
Time (h)	Average concentration (nmol/g)	Average concentration (nmol/g)	Standard deviation (nmol/g)	Average concentration (nmol/g)	Average concentration (nmol/g)	Standard deviation (nmol/g)
0.00	2.05	0.00	0.54	22.2	0.00	3.30
0.50	2.21	1.53	1.00	25.8	16.7	0.97
2.00	1.41	1.03	0.15	17.1	15.3	2.60
6.00	0.57	0.50	0.17	5.36	4.96	0.21
12.00	0.12	0.11	0.01	1.11	1.00	0.14
24.00	0.00	0.00	0.00	0.03	0.02	0.01

Table 3: Parameter values for the semi physiologically based pharmacokinetic model to simulate accumulation in the brain

Two-compartment model	Abbreviation	Value	Source
Apparent plasma volume (L)	V_{plasma}	0.01	Fitted
Plasma to peripheral transfer constant (h^{-1})	K_{12}	2.4	Fitted
Peripheral to plasma transfer constant (h^{-1})	K_{21}	1.21	Fitted
Elimination constant (h^{-1})	K_{el}	1.39	Fitted
Added brain compartment			
Brain volume fraction (fraction of body weight)	V_{BrF}	0.0165	Brown et al. [30]
Vascular volume fraction (fraction of compartment)	V_{Brvf}	0.03	Brown et al. [30]
Cardiac oupout (L/h)	Q_C	0.8388	Brown et al. [30]
Plasma flow in brain as fraction of cardiac output	Q_{BrF}	0.033	Brown et al. [30]
Brain:plasma Partition coefficient	P_{Br}	6.9	Estimated [31]
		0.06	Fitted
Permeability area product (L/h)	PA	1.1×10^{-5}	Fitted

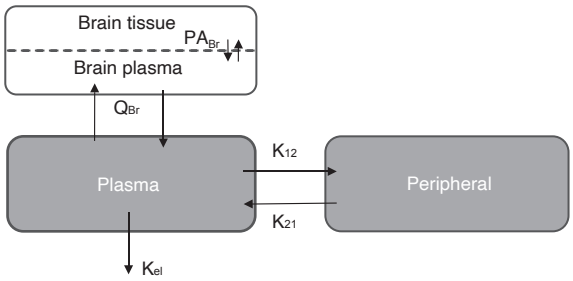
Brain tissue
PA_Br
Brain plasma
Q_Br
K12
Plasma
Peripheral
K21
Kel

Figure 1

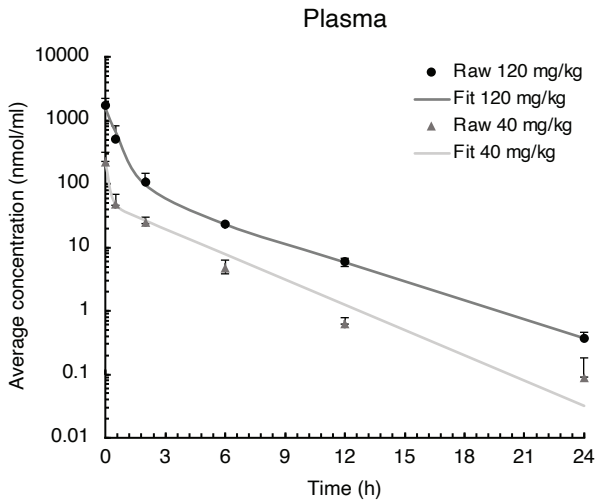
Plasma
Raw 120 mg/kg
Fit 120 mg/kg
Raw 40 mg/kg
Fit 40 mg/kg
Average concentration (nmol/ml)
10000
1000
100
10
1
0.1
0.01
0
3
6
9
12
15
18
21
24
Time (h)

Figure 2

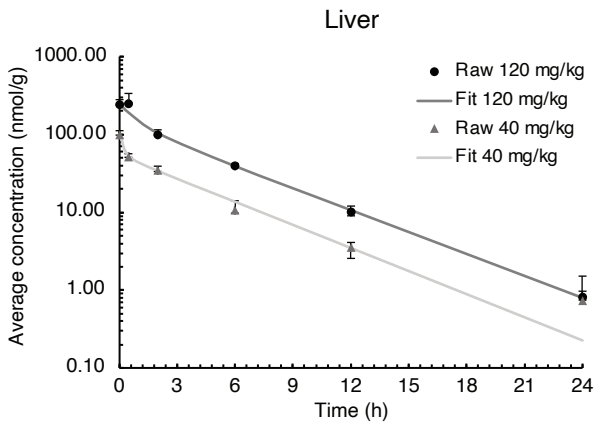
Liver
Average concentration (nmol/g)
1000.00
100.00
10.00
1.00
0.10
0
3
6
9
12
15
18
21
24
Time (h)
Raw 120 mg/kg
Fit 120 mg/kg
Raw 40 mg/kg
Fit 40 mg/kg

Figure 3

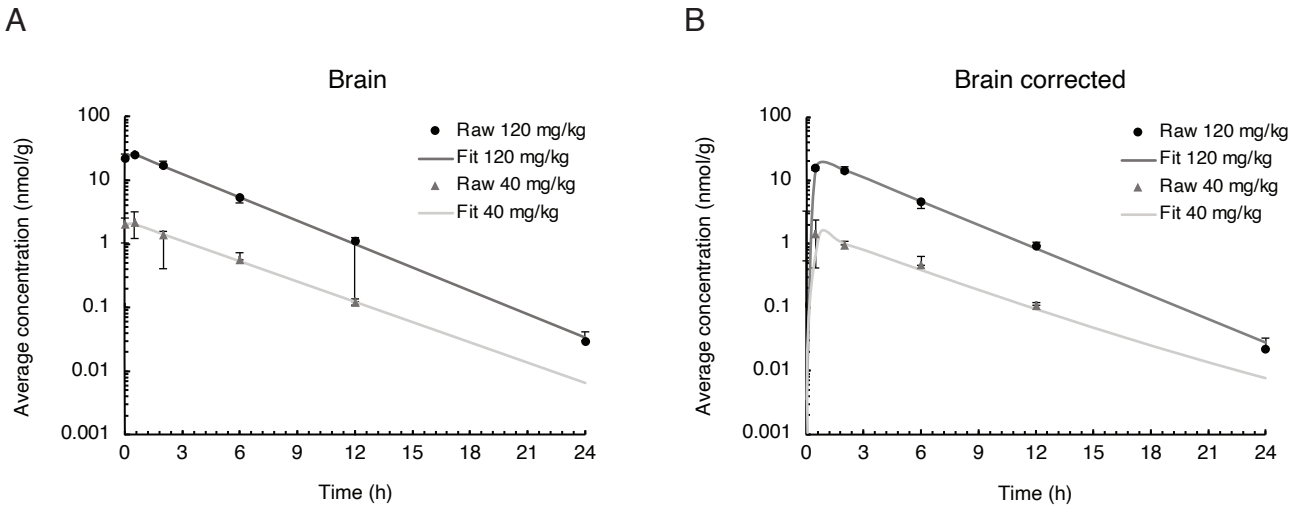
A
Brain
Average concentration (nmol/g)
100
10
1
0.1
0.01
0.001
0
3
6
9
12
15
18
21
24
Time (h)
Raw 120 mg/kg
Fit 120 mg/kg
Raw 40 mg/kg
Fit 40 mg/kg
B
Brain corrected
Average concentration (nmol/g)
100
10
1
0.1
0.01
0.001
0
3
6
9
12
15
18
21
24
Time (h)
Raw 120 mg/kg
Fit 120 mg/kg
Raw 40 mg/kg
Fit 40 mg/kg

Figure 4

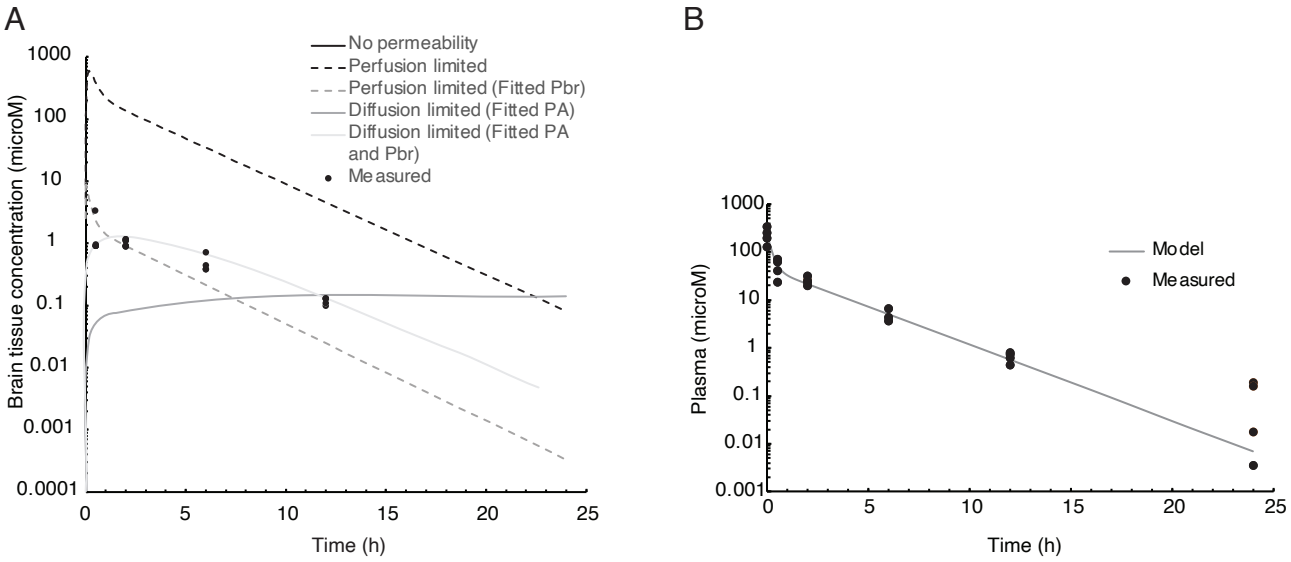
A
No permeability
Perfusion limited
Perfusion limited (Fitted Pbr)
Diffusion limited (Fitted PA)
Diffusion limited (Fitted PA and Pbr)
Measured
Brain tissue concentration (microM)
1000
100
10
1
0.1
0.01
0.001
0.0001
0
5
10
15
20
25
Time (h)
B
Model
Measured
Plasma (microM)
1000
100
10
1
0.1
0.01
0.001
0
5
10
15
20
25
Time (h)

Figure 5